

## Upper mantle tectonics: three-dimensional deformation, olivine crystallographic fabrics and seismic properties

Andréa Tommasi<sup>a,\*</sup>, Basil Tikoff<sup>b</sup>, Alain Vauchez<sup>a</sup>

<sup>a</sup> *Laboratoire Tectonophysique, ISTEEM, CNRS/Université de Montpellier II, 34095 Montpellier, Cedex 5, France*

<sup>b</sup> *Geology and Geophysics, University of Wisconsin at Madison, Madison, WI 53706, USA*

Received 12 August 1998; revised version received 9 February 1999; accepted 18 February 1999

---

### Abstract

Forward numerical models are used to investigate the effect of deformation regime on the development of olivine lattice-preferred orientations (LPO) and associated seismic anisotropy within continental deformation zones. LPO predicted to form by pure shear, simple shear, transpression, or transtension are compared to a database comprising ca. 200 olivine LPO from naturally deformed upper mantle rocks. This comparison suggests that simple shear or plane combinations of simple and pure shear are probably the dominant deformation regimes in the upper mantle. Seismic properties, calculated using the modeled olivine LPO, suggest that seismic anisotropy data may carry information on the deformation regimes active in the lithospheric mantle, although not all deformation regimes are characterized by a distinct seismic anisotropy signal. Transtensional deformation in continental rift systems should result in fast S-wave polarization and P-wave propagation directions oblique to the rift trend within the extended lithospheric mantle. Simple shear (wrench) or transpression in vertical deformation zones and pure shear (horizontal extension) result in similar seismic anisotropy. Simple shear or widening–thinning shear may, however, induce obliquity between seismic and magnetotelluric electrical conductivity anisotropy data. Similarly, it is not possible to distinguish between simple shear or lengthening–thinning shear (plane transpression) in horizontal deformation zones (thrusts) and pure shear (vertical contraction/horizontal extension). In all cases, the polarization direction of the fast split S-wave and the fast P-wave direction parallels the flow direction, but the anisotropy for both Pn- and S-waves is lower in horizontal structures than in vertical ones. Finally, several deformations show an isotropic response to SKS and/or Pn waves, suggesting that seismic isotropy does not necessarily imply absence (or heterogeneity) of deformation. There is a good agreement between model predictions and seismic anisotropy data in both transtensional and transpressional zones, suggesting coupled deformation of the crust and mantle. Oblique fast S-wave polarization directions in the East African rift, for instance, may result from an early transtensional deformation in the mantle lithosphere below the rift system. In contrast, most thrust belts display fast S-waves polarized parallel to the trend of the belt. One possible interpretation is that the upper mantle is decoupled from the crust in these areas. © 1999 Elsevier Science B.V. All rights reserved.

**Keywords:** upper mantle; lithosphere; tectonics; anisotropy; numerical models; petrofabrics; transpression; transtension; strike-slip faults; rift zones

---

\* Corresponding author. Fax: +33-6714-3603; E-mail: deia@dstu.univ-montp2.fr

## 1. Introduction

Seismic anisotropy has emerged in the last decade as a unique tool to probe the upper mantle deformation. This anisotropy results essentially from deformation-induced lattice-preferred orientations (LPO) of olivine, the most abundant ( $\sim 70\%$ ) and most deformable mineral in the upper mantle [1,2]. Inference of upper mantle deformation patterns from seismic anisotropy data is therefore strongly dependent on how olivine LPO evolves during flow.

The relationship between LPO and elastic properties of upper mantle rocks is well-known. The direction of polarization of the fast S-wave and the direction of fast propagation for both Rayleigh and P-waves are parallel to the [100] axis of olivine, and the delay time between the two split S-waves is proportional to the thickness and the intrinsic anisotropy of the deformed layer [3]. On the other hand, the relationship between deformation and LPO remains poorly constrained. Analysis of olivine LPO from naturally [1,2] and experimentally deformed peridotites [4,5] suggests that the [100] axis of olivine tends to parallel the flow direction. However, neither the finite strain nor the actual strain history are known for the natural samples and experiments are restricted to simple deformation paths (axial shortening and simple shear).

In nature, deformation regimes are often a combination of simple and pure shear. Plate motions oblique to continental margins, as well as the mechanical anisotropy of continents due to previous deformation episodes, result in transpression or transtension (e.g., [6,7]). However, the lithospheric mantle response to these deformation regimes remains unknown. Numerical models of LPO evolution during deformation of a polycrystal offer an insight into how olivine LPO develops. Although they simulate deformation by dislocation glide only, these models reproduce most olivine LPO patterns measured in naturally and experimentally deformed peridotites [8].

In this paper, we investigate the effect of a three-dimensional deformation on olivine LPO patterns and seismic properties of upper mantle rocks. We use an anisotropic viscoplastic self-consistent model to predict olivine LPO produced by simple deformations: simple shear, pure shear, transpression and

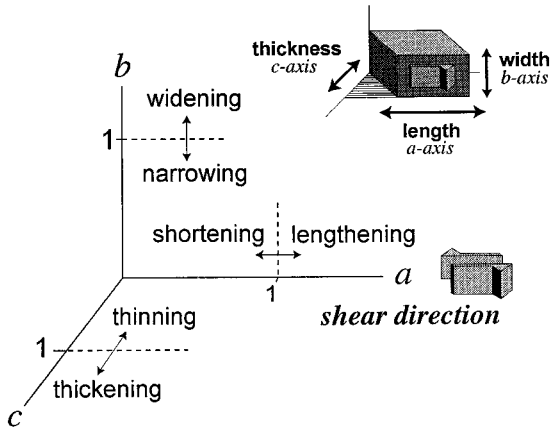
transtension. Modeled LPO patterns are compared to a collection of 200 olivine LPO of peridotites from different geodynamic environments [9]. We use the modeled LPO to calculate the seismic anisotropy associated with each deformation and discuss whether seismic anisotropy data, eventually associated with magnetotelluric soundings, allow discrimination between different deformations within the upper mantle.

## 2. Kinematic model

The kinematic models utilize the concept of three-dimensional reference deformations [10]. These are idealized, volume-conserving deformations with a monoclinic symmetry. Each reference deformation is defined as a simultaneous combination of a simple-shear and a coaxial deformation. This decomposition has the advantage of emphasizing boundary conditions (e.g., transpression) and the finite strain geometry.

The kinematic axes  $a$ ,  $b$ ,  $c$  are determined by the orientation of the simple-shear component of deformation. The  $a$ -axis is parallel to the movement direction, the  $b$ -axis lies in the shear plane and is the rotation axis, and the  $c$ -axis is the normal to the shear plane (Fig. 1). The coaxial component of the deformation is also defined with respect to these axes. Following Tikoff and Fossen [10], we describe the coaxial components based on the three orientations of a shear zone, i.e., length, width, and thickness. The length of the shear zone lies along the  $a$ -axis, the width along the  $b$ -axis, and the thickness along the  $c$ -axis (Fig. 1). A coaxial component parallel to the  $a$ -axis either lengthens or shortens the shear zone, a coaxial component parallel to the  $b$ -axis widens or narrows, and a coaxial component parallel to the  $c$ -axis thickens or thins. These terms relate only to the kinematic axes of the shear zone, and do not have a predetermined orientation in space.

In this study, we investigate four basic deformation types: lengthening–thinning shear (plane transpression), widening–thinning shear ('classical' transpression [11]), thickening–narrowing shear ('classical' transtension), and thickening–shortening shear (plane transtension). Velocity gradient tensors  $\mathbf{L}$  are calculated from an assumed final deformation [12].



### normal to the shear plane

Fig. 1. Orientation of the kinematic axes  $a$ ,  $b$ ,  $c$  relatively to the simple-shear component of deformation for a wrench and a thrust zone. The coaxial component of the deformation — pure shear, flattening, or constriction — is also defined with respect to these axes. It is described based on the three orientations of a shear zone, i.e., length, width, and thickness.

To describe the relative strength of simple-shear and coaxial components, we discount the possibility of external spin and use the kinematic vorticity number ( $W_k$ ).  $W_k$  records the rotation rate relative to the stretching rate at a point in space [13]. Simple shear induces an equal amount of rotation and stretching ( $W_k = 1$ ). A coaxial deformation has no rotation ( $W_k = 0$ ). Although  $W_k$  is defined only for infinitesimal deformations, it may be calculated for a bulk deformation if the three-dimensional deformation remains constant through time [14]. For each deformation regime, we tested the effect of varying the relative amount of coaxial components and simple-shear components ( $W_k$  from 0.75 to 0.975).

### 3. Olivine lattice-preferred orientation and seismic anisotropy modeling

Olivine lattice-preferred orientations developed under different deformation regimes are predicted using an anisotropic viscoplastic self-consistent model (VPSC) [15]. In contrast to classical lower [16] or upper bound [17] approaches, that impose, respectively, homogeneous stress or strain within the aggregate,

the VPSC approach allows both the microscopic stress and strain rate to differ from the corresponding macroscopic quantities. Strain compatibility and stress equilibrium are ensured at the aggregate scale.

At the grain scale, deformation is accommodated by dislocation glide only; other deformation mechanisms like dynamic recrystallization are not taken into account. The shear rate in a slip system 's' is related to the local deviatoric stress tensor  $\mathbf{s}$  by a viscoplastic law:

$$\dot{\gamma}^s = \dot{\gamma}_0 \left( \frac{\tau_r^s}{\tau_0^s} \right)^{n^s} = \dot{\gamma}_0 \left( \frac{r_{ij}^s s_{ij}}{\tau_0^s} \right)^{n^s} \quad (1)$$

where  $\dot{\gamma}_0$  is a reference strain rate, taken as  $1 \text{ s}^{-1}$ , and  $n^s$ ,  $\tau_r^s$ , and  $\tau_0^s$  are, respectively, the stress exponent, the resolved shear stress, and the critical resolved shear stress for the system 's', whose orientation relative to the macroscopic axes is expressed by its Schmid tensor  $\mathbf{r}^s$ . The potentially active slip systems for olivine, their critical resolved shear stresses, and their stress exponent (Table 1) are evaluated from microscopic studies of naturally and experimentally deformed peridotites and from single-crystal deformation experiments [18].

The problem lies in the calculation of a microscopic state ( $\mathbf{s}$ ,  $\dot{\epsilon}$ ) for each grain, whose volume average determines the response of the polycrystal ( $\bar{\mathbf{S}}$ ,  $\bar{\mathbf{D}}$ ). The '1-site' approximation [19] is used in the anisotropic VPSC formulation; the influence of neighboring grains is not taken into account. In-

Table 1  
Slip systems data

Slip system	Critical resolved shear stress $\tau_0^a$	Stress exponent $n$
(010)[100]	1	3.5
(001)[100]	1	3.5
(010)[001]	2	3.5
(100)[001]	3	3.5
{011}[100]	4	3.5
{031}[100]	4	3.5
{110}[001]	6	3.5
{111}[110] and {111}[011] <sup>b</sup>	500	3.5

<sup>a</sup> Normalized relative to  $\tau_0$  (010)[100].

<sup>b</sup> Since olivine displays only three independent slip systems, 'complementary' pyramidal systems have to be introduced in the Taylor calculation of the initial solution (first iteration), but they are not used in the subsequent VPSC iterations.

interactions between each grain and its surroundings are successively replaced by the interaction between an inclusion with similar lattice orientation and an infinite homogeneous equivalent medium (HEM), whose behavior is the weighted average of the grains behavior. This leads to:

$$\dot{\varepsilon}_{ij} - D_{ij} = -\alpha \tilde{\mathbf{M}}_{ijkl} (s_{kl} - \bar{\Sigma}_{kl}) \quad (2)$$

where  $\tilde{\mathbf{M}}$  is the interaction tensor and  $\alpha$  is a constant used to parameterize the interaction between grains and the HEM.  $\alpha = 0$  corresponds to the upper bound model and  $\alpha = \text{infinity}$  to the lower bound model. Comparison between model results and olivine LPO measured in naturally and experimentally deformed peridotites indicate that the best predictions are yielded by VPSC models with relaxed strain compatibility ( $\alpha > 1$ ) [8]. In the following simulations,  $\alpha = 10$ .

Simulations are run for aggregates with a spherical initial grain shape and an initially random orientation distribution of 1000 olivine grains. The strain history is imposed by prescribing a constant macroscopic velocity gradient tensor  $\mathbf{L}$  (Fig. 3) and a time increment,  $d\tau$ , set to achieve an equivalent strain of 0.025 in each deformation step. The equivalent strain is defined as [19]:

$$\varepsilon_{\text{eq}} = \int \mathbf{D}_{\text{eq}}(\tau) d\tau \quad (3)$$

where the Von Mises equivalent strain rate is:

$$\mathbf{D}_{\text{eq}} = \sqrt{2/3 \mathbf{D}_{ij} \mathbf{D}_{ij}} \quad (4)$$

The elastic properties of the aggregate are calculated as a Voigt–Reuss–Hill average of the olivine elastic stiffness coefficients ( $C_{ijkl}$ ) [20] over all crystal orientations and the Christofel equation is used to predict velocities and polarization directions for P- and S-waves propagating in any direction relative to the structural fabric [21].

#### 4. Model results

Preferred orientations of [100], [010], and [001] axes developed in pure-shear, simple-shear, flattening, transpressional, and transtensional deformations are presented in Figs. 2 and 3. LPO evolution with progressive strain is only presented for simple shear

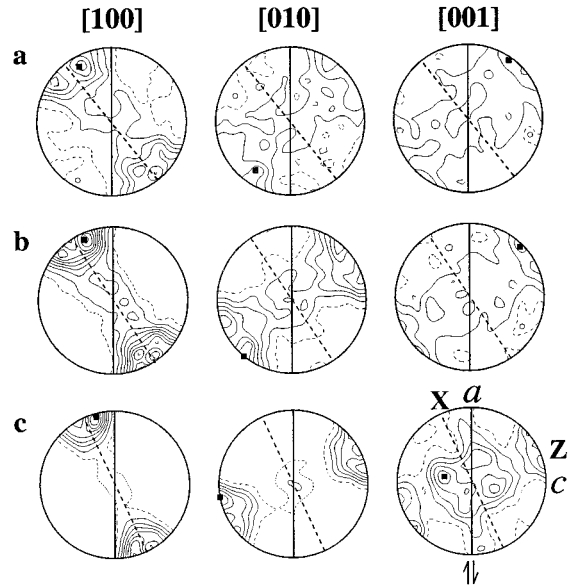


Fig. 2. LPO evolution in an olivine aggregate submitted to dextral simple shear. (a)  $\varepsilon_{\text{eq}} = 0.25$  ( $\gamma = 0.43$ ). (b)  $\varepsilon_{\text{eq}} = 0.5$  ( $\gamma = 0.87$ ). (c)  $\varepsilon_{\text{eq}} = 1$  ( $\gamma = 1.73$ ). Equal-area projection, lower hemisphere, 1000 grains. Contours at 0.5% intervals, except for [100] and [010] in (c) that are contoured at 1% intervals. Both the shear plane ( $ab$  plane; full line) and the foliation ( $XY$  plane; dashed line) are vertical; the shear direction ( $a$ ) and lineation ( $X$ ) are horizontal within these planes. Maximum density is marked by a full square.

(Fig. 2), since strain accumulation during coaxial deformation merely intensifies the LPO patterns. To allow comparison between different strain regimes, all LPO are shown for an equivalent strain of 1. For transpression and transtension, simulations using different proportions of simple and pure shear ( $0.75 \leq W_k \leq 0.975$ ) were run, but we only discuss the results for those runs that produced distinct LPO patterns.

The anisotropy for both P- and S-waves propagating with different directions relative to the structural fabric bears a close relationship to the LPO (Fig. 3). P-waves propagating parallel to the [100] maximum display the highest velocities and those propagating parallel to the [010] maximum the lowest velocities. P-wave anisotropy depends on the intensity of these LPO maxima and hence on the deformation regime and finite strain. For S-waves, the fast split S-wave is polarized in the plane that contains both the propagation direction and the [100] maxima. The difference

in velocity between the two split S-waves depends on the intrinsic anisotropy, which in turn depends on the LPO intensity and on the direction of wave propagation relative to the structural frame. The highest anisotropy values are obtained for S-waves propagating parallel to the flow plane, but at high angle (50–70°) from the flow direction. The lowest anisotropies are obtained for S-waves propagating either at low angles to the flow direction or normal to the flow plane, depending on the LPO pattern. For both P- and S-waves, anisotropy does not depend linearly on finite strain; it increases quickly for low strains ( $\varepsilon_{\text{eq}} \leq 3$ ) and then it tends to a limiting value that depends on the LPO pattern and sample composition [8].

Note that in Fig. 3, seismic properties are calculated for a dunite (100% olivine). Presence of other upper mantle minerals does not affect the anisotropy pattern, but it weakens both P- and S-waves anisotropies [3]. For a typical upper mantle composition (70% olivine, 30% enstatite), maximum anisotropy values are ca. 8% for S-waves and 12% for P-waves [3,8].

#### 4.1. Simple shear

At an equivalent strain of 0.25, a characteristic simple-shear LPO pattern is already developed (Fig. 2). [100] axes show a bimodal maximum symmetric to the XY plane of the finite strain ellipsoid. [010] and [001] form crossed-girdles at high angle to X. [010] displays a bimodal maximum close to Z and [001] shows a weak maximum close to Y. With increasing strain, the [100] maximum that lies in-between the shear and finite elongation directions is progressively strengthened. The [010] maximum normal to the shear plane is also intensified. The LPO tends to a single maxima pattern, that displays a monoclinic symmetry relative to the foliation and lineation.

A similar LPO evolution is observed in experimental simple-shear deformation of dunites at 1200°C [5]. At 1300°C, however, dynamic recrystallization accelerates LPO evolution; after a shear strain of 1, samples are largely recrystallized and display [100] and [010] single maxima parallel to the shear direction and normal to the shear plane, respectively. Single maximum [100] patterns slightly asymmetric relative to the foliation (XY plane) are the

most common LPO patterns in naturally deformed peridotites [9], especially in those from ophiolitic massifs, that are supposed to have deformed dominantly by simple shear [22]. These single maximum [100] patterns show a continuous variation between two equally common end-members: (i) single maxima distributions of [010] parallel to the *c*-axis and [001] parallel to the *b*-axis; and (ii) girdle distributions of [010] and [001] normal to the *a*-axis. The first pattern, characteristic of experimentally sheared peridotites, results from dominant slip on (010)[100]. The second, ‘axial [100]’ pattern results from slip on two or more of the {0kl}[100] systems. Both patterns are reproduced in the simulations, depending on the imposed strain compatibility. ‘Axial [100]’ patterns occur in models with  $\alpha \geq 10$  and (010)[100] patterns in models with  $\alpha = 1$  [8].

VPSC simulations of LPO development in simple shear reproduce the main characteristics of LPO patterns of naturally and experimentally sheared peridotites, but, because they do not simulate dynamic recrystallization, the models display a slower rotation of the [100] maximum towards the shear direction. Yet, at a shear strain of 1, the misorientation between model predictions and the measured LPO for a highly recrystallized peridotite is less than 15°.

Simple shear LPO leads to strong anisotropy for both P- and S-waves (Fig. 3). The fastest direction of propagation for P-waves as well as the polarization of the fast S-wave depend on the deformation intensity. At low shear strains, both directions are oblique to the shear direction. With increasing shear, the fastest direction of propagation for P-waves and the polarization of the fast S-wave rotate towards the shear direction. For  $\varepsilon_{\text{eq}} \geq 1$ , P-waves propagating close to the shear direction are the fastest, and those propagating roughly normal to the shear plane are the slowest. Independently of their direction of propagation, fast S-waves are polarized sub-parallel to the shear direction. The maximum and minimum S-wave anisotropy is detected by waves propagating within the *ab*-plane at high angles and low angles to the *a*-axis, respectively.

#### 4.2. Axial shortening

Simulation of LPO development during axial shortening shows that [010] tends to concentrate in a

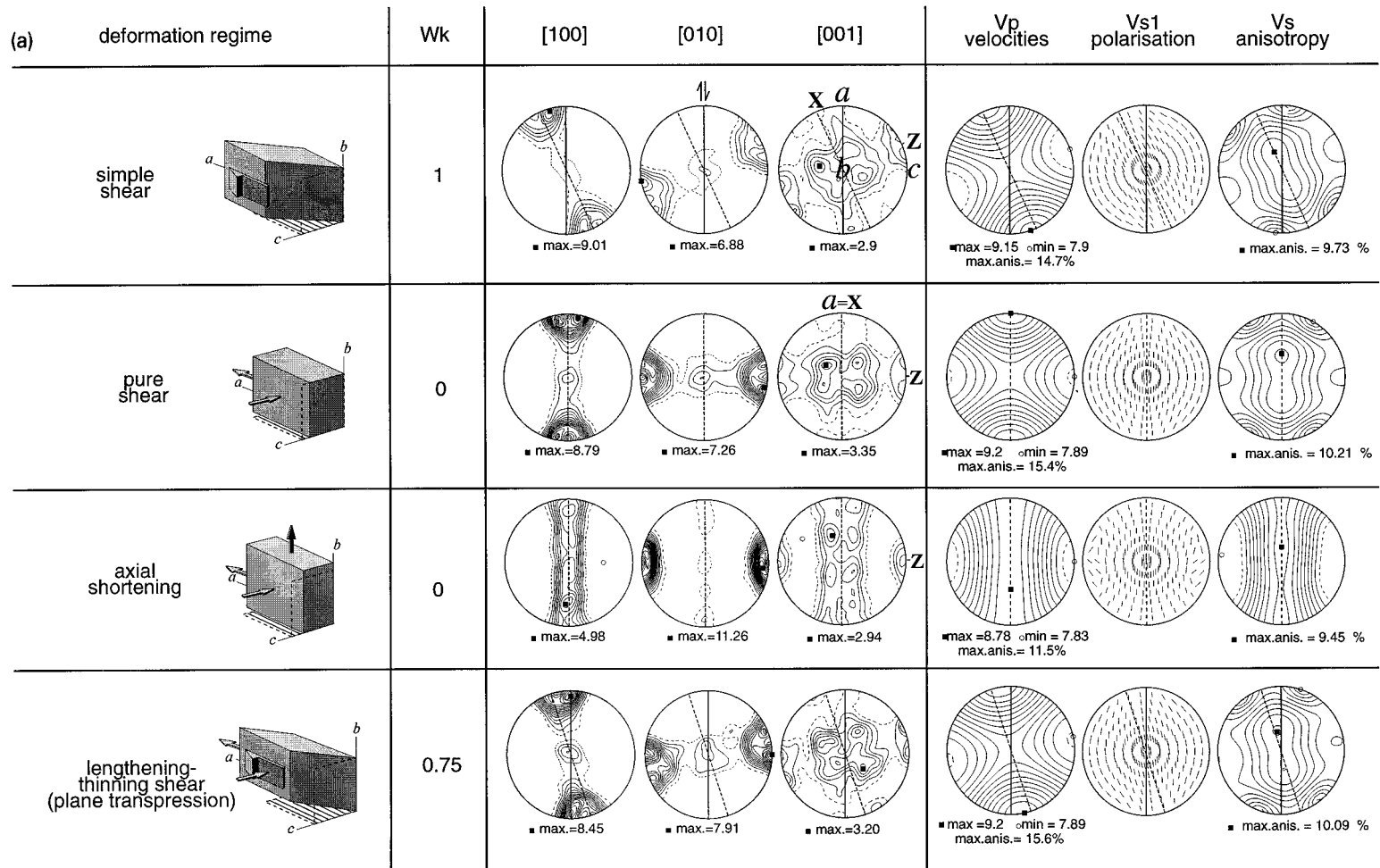


Fig. 3. LPO and seismic properties for olivine aggregates submitted to dextral simple shear, pure shear, axial compression, widening–thinning, lengthening–thinning, thickening–narrowing, and thickening–shortening shear at an equivalent strain of 1. Equal-area projections, lower hemisphere, 1000 grains. LPO and S-waves anisotropy are contoured at 1% intervals, P-wave velocities at 0.1 km/s intervals. Both the shear plane ( $ab$  plane; full line) and the foliation ( $XY$  plane; dashed line) are vertical; the shear direction ( $a$ ) and lineation ( $X$ ) are horizontal within these planes.

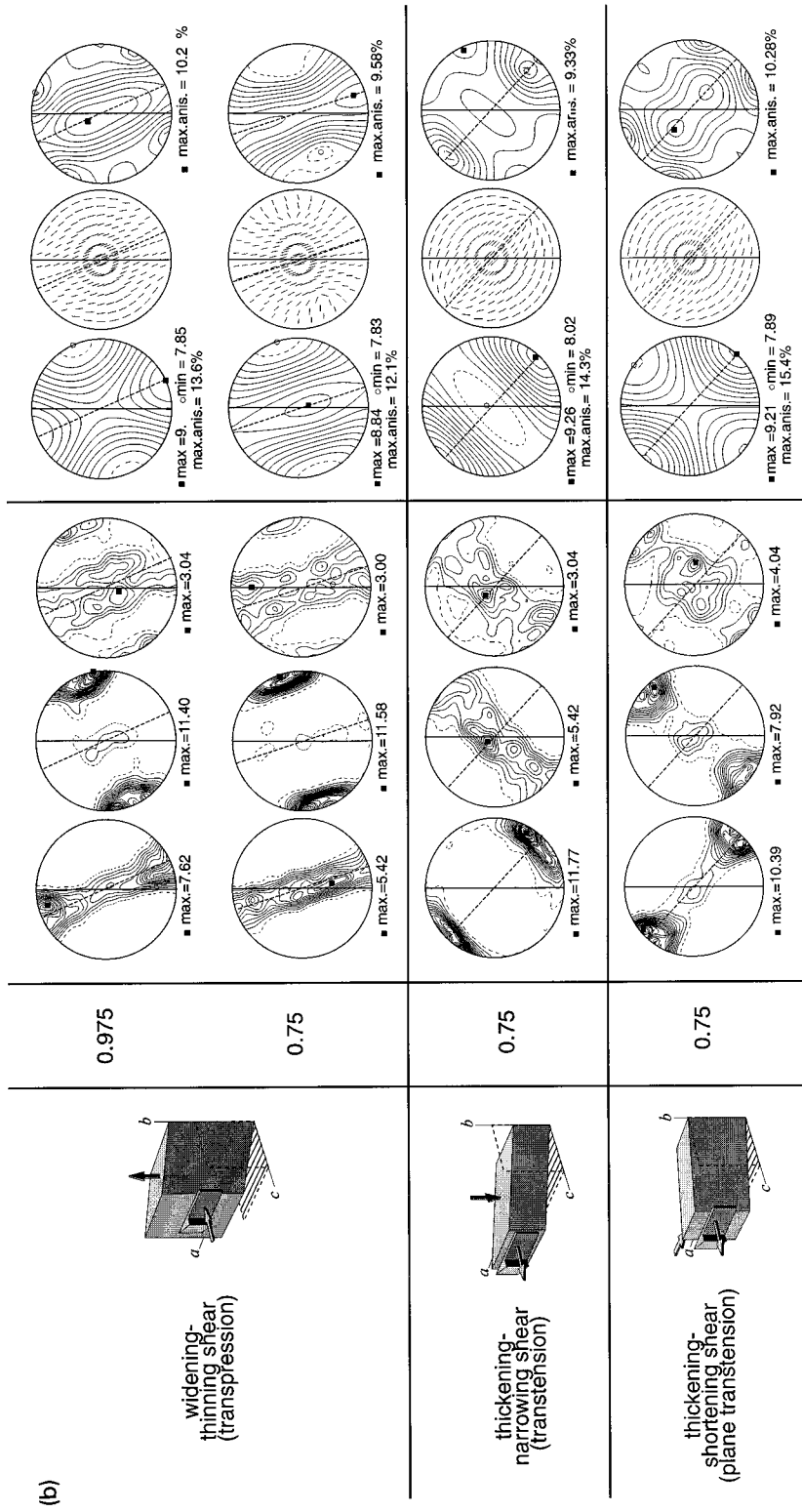


Fig. 3 (continued).

small circle around the shortening direction ( $Z = c$ ), while [100] and [001] form girdles at high angle to this direction. This LPO displays an axial symmetry relatively to the shortening direction and it will be referred to hereafter as the ‘axial [010]’ pattern.

Dunitic aggregates subjected to axial compression under experimental conditions also develop ‘axial [010]’ patterns [4]. However, modeled LPO differ from those observed in the experiments by their relative organization of [100] and [001]. In experimentally deformed samples, [001] forms a girdle almost normal to the shortening direction and the [100] distribution is more diffuse. In numerical simulations, [100] concentrates in a girdle normal to the shortening direction and [001] shows a more diffuse distribution. This discrepancy between observed and modeled LPO may be explained by activation of different slip systems in the experiments and simulations. Critical resolved shear stresses in our models simulate high-temperature deformation characterized by dominant [100] slip, whereas, in the experiments, the low-temperature {110}[001] system was significantly activated [4]. Activation of low-temperature slip systems at temperatures of 1200–1300°C is probably due to the high strain rates and dry conditions of the experiments.

Natural deformation occurs at much lower strain rates (e.g.,  $10^{-14}$  s $^{-1}$ ), for which the dominant slip direction is [100]. Indeed, ‘axial [010]’ patterns in naturally deformed peridotites are invariably characterized by a better orientation of [100] than [001]. Thus we infer that the models reproduce correctly olivine LPO development due to axial shortening in the upper mantle. Yet, ‘axial [010]’ LPO patterns, most common in peridotites from cratonic environments, represent less than 15% of the database [9]. This observation suggests that axial shortening is not common in the upper mantle. However, our sampling of the lithospheric mantle (through tectonic processes or magmatism) is incomplete and the database may not be fully representative of the upper mantle deformation.

Olivine aggregates deformed by axial shortening display lower P- and S-waves anisotropies than aggregates deformed by simple shear. P-waves propagating within the foliation display the fastest velocities and those propagating parallel to the shortening direction the slowest velocities. No P-wave

anisotropy, but maximum S-wave anisotropy will be observed for waves propagating within the foliation plane. Fast S-waves are polarized normal to the shortening direction, except for those propagating normal to the foliation. However, such a propagation direction results in a very weak anisotropy and these polarizations probably cannot be detected.

#### 4.3. Pure shear

Pure shear produces a LPO pattern with an orthorhombic symmetry: [010] axes tend to concentrate in a small circle around the shortening direction ( $Z = c$ ) and [100] axes tend to align towards the elongation direction ( $X = a$ ). This LPO pattern is similar to those displayed by dunites deformed under experimental conditions that approach pure shear [23]. Experimentally deformed samples, however, show a faster LPO development, interpreted by Avé Lallemant [23] as a result of dynamic recrystallization.

Orthorhombic LPO patterns symmetric to the foliation plane are observed in naturally deformed peridotites, but they are less common than asymmetric ones. This suggests that in the lithospheric mantle, as in the crust, simple shear or combinations of simple and pure shear are probably the dominant deformation regimes.

Seismic properties of olivine aggregates deformed by pure shear are very similar to those of aggregates deformed by simple shear, except that they do not rotate with increasing strain. Fast and slow directions of propagation for P-waves and of polarization for S-waves are always symmetric relative to the foliation and lineation. At similar strains, pure shear leads to a slightly stronger anisotropy for both P- and S-waves.

#### 4.4. Lengthening–thinning shear (plane transpression)

Lengthening–thinning shear results in development of single maxima LPO patterns intermediate between pure and simple shear ones. LPO evolution is characterized by a faster rotation of the [100] axes towards the  $a$ -axis and of the [010] axes to the  $c$ -axis than simple shear. However, LPO measurements in experimentally deformed dunites [5]

suggest that dynamic recrystallization produces parallelism between [100] and the shear direction is attained at low shear strains ( $\gamma \approx 1$ ) even in simple shear. Moreover, in lengthening–thinning shear, the foliation also rotates faster towards the shear plane. Thus it is probably not possible to distinguish LPO developed during lengthening–thinning shear from those formed through simple shear or pure shear. Accordingly, aggregates deformed in these three deformation regimes show similar seismic properties.

#### 4.5. Widening–thinning shear (classical transpression)

In widening–thinning shear, even a very low amount of pure shear ( $W_k = 0.975$ ) tends to transform the simple shear LPO into a flattening one. For  $0.75 \leq W_k \leq 0.9$ , [010] forms a small girdle oblique to the shortening direction; this obliquity decreases with increasing finite strain or proportion of pure shear. [100] and [001] form complete to incomplete girdles at high angle to the shortening direction. For  $W_k = 0.975$ , [100] axes display a strong maximum close to the  $a$ -axis and [001] a weak maximum near the  $b$ -axis. For higher proportions of pure shear ( $W_k \geq 0.75$ ), the stronger [100] maximum shifts towards the  $b$ -axis. This reorganization of the [100] maxima also occurs at  $W_k = 0.9$ , but at higher finite strains. It corresponds to a switch of the finite elongation direction  $X$  from sub-parallel to the  $a$ -axis to sub-parallel to the  $b$ -axis, in agreement with the observation of lineations normal to the shear direction in transpressional zones [24]. However, as already stated, ‘axial [010]’ LPO patterns are rare in naturally deformed peridotites, suggesting that neither axial shortening nor widening–thinning shear are common in the upper mantle.

Seismic properties of aggregates submitted to widening–thinning shear depend on the relative strength of the simple shear and coaxial components of the deformation. For very low amounts of pure shear (the  $W_k = 0.975$ ), patterns are very similar to those displayed by olivine polycrystals deformed by simple shear, but the anisotropy is lower. For higher amounts of pure shear ( $W_k = 0.75$ ), however, the fastest direction of P-wave propagation becomes parallel to the  $b$ -axis. Large S-wave anisotropy is recorded by waves propagating within the folia-

tion, the highest anisotropy is observed for waves propagating close to the lineation. No anisotropy is observed for S-waves propagating at high angle to the shear plane. For other propagation directions, the fast S-wave is polarized at low angle to the shear direction.

#### 4.6. Thickening–narrowing shear (classical transtension)

In thickening–narrowing shear, the finite strain axes  $X$  and  $Z$  are strongly oblique to the  $a$ - and  $c$ -axes. Consequently, thickening–narrowing shear results in an ‘axial [100]’ pattern oblique to the macroscopic shear: [100] develops a strong maximum sub-parallel to the lineation, whereas [010] and [001] form girdles sub-parallel to the foliation. As for widening–thinning shear, the obliquity of both LPO and finite strain directions relative to the kinematic axes depends on the proportion of pure and simple shear and on the finite strain.

‘Axial [100]’ patterns symmetrical or slightly asymmetrical relative to the foliation are common in naturally deformed peridotites [9]. However, such patterns may also develop in simple shear if olivine deforms by multislip on  $\{0kl\}[100]$  systems [8]. Thus, in mantle xenoliths, thickening–narrowing shear cannot be distinguished from simple shear. However, when information on the kinematic axes is available, LPO developed in thickening–narrowing shear may be easily distinguished from those formed by simple shear.

Aggregates deformed by thickening–narrowing shear display characteristic seismic properties. Their anisotropy is high. P-waves propagating close to the lineation are the fastest. The lowest P-wave velocities are recorded in a plane normal to this direction. For most propagation directions, fast S-waves are polarized oblique to the shear direction. High S-wave anisotropy is recorded for S-waves propagating at high angle to the foliation. Low S-wave anisotropy are detected by waves propagating close to the lineation.

#### 4.7. Thickening–shortening shear (plane transtension)

Thickening–shortening shear produces orthorhombic LPO patterns similar to those developed

through simple shear, but, in this case, the obliquity between the LPO and the kinematic axes is much higher. As for thickening–narrowing shear, [100] axes develop a strong maximum oblique to the  $a$ -axis. This maximum is rotated clockwise from the lineation, in agreement with the imposed dextral shear.

LPO produced by thickening–shortening shear, simple shear, or lengthening–thinning shear may only be distinguished if information on the kinematic reference frame (shear plane and/or direction) is available. Thus we cannot use the olivine LPO database of xenoliths to evaluate if thickening–shortening shear occurs in the upper mantle.

Aggregates deformed by thickening–shortening shear display a strong anisotropy for both P- and S-waves. The fastest P-waves propagate close to the lineation. Fast S-waves are polarized obliquely to the shear direction, independent of their propagation direction. The highest S-wave anisotropy is detected by S-waves propagating within the foliation at high angle to the lineation.

## 5. Seismic anisotropy signature of continental deformation zones

Shear wave splitting and Pn anisotropy offer complementary information on the deformation of the lithospheric mantle. Splitting of core S-waves provides robust estimations of azimuthal anisotropy with a lateral resolution of ca. 50 km, but it lacks vertical resolution. Pn-waves, in contrast, sample only the uppermost mantle, but, like any propagation anisotropy data, their interpretation is hindered by a trade-off between heterogeneity and anisotropy. Polarization and azimuthal anisotropies of surface waves also provide information on lithospheric mantle structure, but they have poor lateral resolution (350–1000 km depending on frequency). They cannot therefore resolve short wavelength variations in the deformation field that may occur within the lithospheric mantle.

Further constraints on the lithospheric mantle fabric are provided by measurements of electrical conductivity anisotropy through magnetotelluric soundings, since conductivity anisotropy in mantle rocks is probably related to conductive films along ori-

ented grain boundaries (i.e., the foliation [25]). In areas where both magnetotelluric soundings and seismic anisotropy data are available, like the Superior Province of Canada and the Appalachians, the direction of maximum conductivity is roughly parallel to the fast S-wave polarization [26,27]. In addition, the source of electrical conductivity anisotropy may be located vertically, because, like surface waves, magnetotelluric waves display a frequency-dependent penetration.

In the next paragraphs, we investigate the seismic anisotropy signal generated by nearly vertically incident core S-waves (e.g., SKS) and horizontally propagating Pn-waves in a variety of geodynamic environments. The effect of the deformation regime on the seismic anisotropy signal is analyzed for vertical and horizontal deformation zones within the lithospheric mantle. The seismic anisotropy associated with a deformation zone of general orientation may be inferred from Fig. 3. However, since core S-waves arrive in a cone at 5–20° from the vertical, S-wave splitting for inclined structures will depend on the wave back-azimuth, showing a 180° periodicity [28].

### 5.1. Major strike-slip and transpressional faults

Observation of Moho offsets, variations in crustal structure, and diffractions in seismic profiles across continental-scale strike-slip shear zones suggests that these faults penetrate the entire crust and continue in the upper mantle [29]. Within these shear zones, a core S-wave propagates close to the  $b$ -axis (vertical). Pn anisotropy results from velocities variations between Pn waves propagating in different directions within the  $ac$  plane.

Vertically structured domains deforming by simple shear, transpression, or pure shear will display fast S-waves polarized roughly parallel to the structural trend and strong P- and S-waves anisotropies (Fig. 3). Simple shear may only be identified in shear zones displaying a strain gradient from the borders to the center, that will show a continuous rotation of fast P-wave propagation and S-wave polarization directions from oblique to parallel to the shear zone. Widening–thinning shear with high proportions of pure shear and/or high finite strains will be characterized by a lower Pn anisotropy, since a horizontally

propagating P-wave will not sample the fastest propagation direction.

Core S-waves splitting data above major transcurrent faults invariably display fast S-waves polarization parallel to the faults' trace at the surface and high delay times [30], suggesting that the entire lithospheric mantle is deformed. The rotation of the fast S-wave polarization in the vicinity of these faults suggests that the upper mantle tectonic fabric is curved into parallelism to the shear zone (e.g., the Great Glen fault in the Scottish Caledonides [31], the Kunlun [32] and the Altyn Tagh [33] active faults in Tibet, the Martic line in the eastern U.S. [34], and the San Andreas transform [28]). Pn anisotropy measurements in the San Andreas region indicate that Pn-waves propagating parallel to the fault trend are the fastest [35]. These observations as well as those in transform boundaries submitted to transpression, like the Caribbean [36] and New Zealand [37], are in good agreement with our model predictions for wrench and transpressional upper mantle deformation.

In addition, simple-shear deformation in the upper mantle may be characterized by an obliquity between fast directions for seismic and electrical anisotropies [26]. Such an obliquity is, for instance, observed in the Canadian Abitibi belt; it is interpreted as resulting from dextral shearing within the lithospheric mantle [26]. However, experimental data suggest that parallelism between the olivine [100] axis and the shear direction is only attained after a significant amount of recrystallization; weakly recrystallized samples display [100] maxima at 20–45° to the shear direction [5]. In addition, the foliation tends to parallel the shear plane at high strains. Thus obliquity between seismic and electrical (magnetotelluric) anisotropy data should not be observed in upper mantle domains submitted to very low (electrical and seismic fast directions oblique to the shear zone) or high shear strains (both directions parallel the shear zone).

### 5.2. Transpressional belts

Fast S-wave polarization and P-wave propagation directions parallel to the regional structural trend are not restricted to the vicinity of major strike-slip faults. The consistency of this parallelism over

large orogenic domains, like the eastern U.S. [34], the Pyrenees [38,39], and the Ribeira–Brasília Neoproterozoic belts in southern Brazil [40,41], cannot be explained by an upper mantle deformation localized within one or a few belt-parallel vertical shear zones [6]. LPO development during a pre-orogenic rifting episode [42] also cannot explain belt-parallel anisotropy over such wide regions. The observed belt-parallel SKS splitting may, however, be explained if the lithospheric mantle deformed by transpression. Transpression in the crust is usually characterized by partitioning of the deformation between wrench and thrust domains (e.g., the Appalachians [43]). In the upper mantle, transpression may be either homogeneous or partitioned; both deformations give rise to similar seismic signatures.

### 5.3. Thrust belts

Within a horizontal deformation zone, core S-waves propagate normal to both the flow plane and flow direction, and Pn anisotropy results from azimuthal velocity variations within the flow plane. For lengthening–thinning or simple shear, fast S-waves should be polarized parallel to the shear direction, i.e., normal to the belt (Fig. 3). In addition, for similar deformed layer thicknesses, delay times between split S-waves should be lower than those expected over vertical structures (respectively 5% and 9% S-wave anisotropy for a dunite).

Yet, most splitting measurements in thrust belts show fast S-waves polarized parallel to the trend of the belt (e.g., the northern Apennines [44], the Himalayan chain [32,45,46], or the Hercynian belt in central Europe [47]). Fast core S-waves polarized normal to the trend of the belt, i.e., parallel to the direction of thrusting, have only been observed in a few stations in the easternmost Hercynian belt [47], in southeastern Tien Shan [45,46] and in the northern Ribeira belt, Brazil [41].

Belt-parallel fast S-wave polarization and large delay times cannot be produced in subhorizontal deformation zones. In horizontal widening–thinning shear zones, olivine [100] axes tend to align parallel to the *b*-axis for high proportions of pure shear or high finite strain, but, in this case, core S-waves record no anisotropy. The large delay times generally observed in orogenic belts ( $\geq 1$  s) also rule out

horizontal shortening and thickening by pure shear, since it results in a vertical orientation of olivine [100] axis and, hence, in very low delay times, even for a thickened lithosphere. Fast S-wave polarization and fast Pn propagation parallel to the trend of the belt may result from simple shear or transpression in vertical shear zones or uniaxial horizontal shortening (i.e., a flow component parallel to the trend of the belt). This suggests that thrusting may be a minor process in the deformation of the lithospheric mantle and that orogenic domains deforming by thrusting and crustal thickening are often decoupled from the underlying mantle (e.g., the external Pyrenees and Appalachians [38]).

#### 5.4. Continental rifts

Lithospheric extension and continental rifting are usually explained through two simple models: pure shear or simple shear. Both should generate fast S-wave polarization and P-wave propagation directions normal to the trend of the rift. In addition, extension through simple shear should result in development of an inclined shear zone and, hence, in dependence of SKS splitting on the S-wave back-azimuth with a 180° periodicity. Fast S-wave polarizations normal to the trend of the rifts are nevertheless seldom observed.

Focal mechanisms and geodetic studies indicate that most rift systems are submitted to strike-slip faulting as well as extension [48,49]. This suggests that the lithosphere in a continental rift system deforms through thickening–narrowing shear. Our simulations suggest that transtensional shear zones display a characteristic seismological signature: fast S-wave polarization and P-wave propagation directions oblique to the regional structural trend. Fast S-wave polarization directions oblique to the rift direction have been measured in the Rio Grande and Kenya rifts [50,51]. In the central domains of these rift systems, the measured anisotropy probably records both lithospheric and asthenospheric structures [51,52]. However, in the Kenya rift, teleseismic tomographic data suggests that lithospheric thinning is restricted to a narrow channel that roughly follows the surface expression of the rift [53]. The NNE–SSW to NE–SW fast S-wave polarization directions observed outside the rift [51] may thus result from

sinistral transtension within the lithospheric mantle. Focal mechanisms for recent earthquakes suggest that this part of the East African rift is presently deforming by dextral transtension [48], but sinistral shear is inferred to have occurred during the Late Miocene–Early Pliocene [54]. Correlation between seismic anisotropy and the early kinematics of the rift system is coherent with a model of rifting through lithospheric rupture [55], in which the main deformation of the lithospheric mantle occurs during the early stages of rifting.

## 6. Conclusion

Forward numerical models are used to investigate the effect of a three-dimensional deformation on the olivine LPO and the seismic anisotropy within continental deformation zones. Comparison of modeled LPO with olivine LPO from naturally deformed peridotites suggests that simple shear or plane combinations of simple and pure shear are the dominant deformation regimes in the upper mantle. Seismic properties calculated using the modeled LPO show that seismic anisotropy data may carry information on the deformation regimes within the upper mantle, although not all deformation regimes are characterized by a distinct seismic anisotropy signal. Simple shear within vertical deformation zones is characterized by obliquity between seismic and electrical conductivity anisotropies, but only for intermediate strains. Even when the directional parameters of anisotropy are similar, changes in deformation regime may result in variations in the anisotropy intensity. Indeed, short-scale variations in delay time are frequently observed. They may reflect lateral variations in deformation regime. For instance, delay times measured in the northern Ribeira belt (Brazil), where thrusting is dominant, are significantly lower than those observed in the southern domain that deforms by transpression [41].

Transtension is probably the deformation that displays the most characteristic signature: fast S-wave polarization and P-wave propagation directions strongly oblique to the rift trend. The oblique fast S-wave polarizations observed in the external domains of the East African rift may thus result from an early transtensional deformation within the rift

system. The good agreement between model predictions and seismic anisotropy data above strike-slip and transpressional shear zones suggests coupled deformation of the crust and mantle. On the other hand, contractional deformation of the lithospheric mantle in low-angle thrusts is only supported by a few isolated observations. Most collisional belts display fast S-waves polarized parallel to the trend of the belt (normal to the crustal transport direction) and high delay times even in thrust-dominated domains. This suggests that the upper mantle is decoupled from the crust in these areas and displays a flow-component parallel to the trend of the belt.

Finally, our models show that an isotropic response to SKS or Pn waves may be generated by vertical flow, vertical axial shortening, or widening–thinning shear in a subhorizontal deformation zone. However, in those cases, surface waves should still display polarization anisotropy. A joint analysis of surface and body waves may therefore discriminate whether absence of SKS splitting [30] results from a random olivine LPO, a heterogeneous deformation field, or one of these deformations.

## Acknowledgements

We thank D. Mainprice for fruitful discussions on LPO development, R. Lebensohn for providing the anisotropic VPSC code and S. Zhang for making his LPO measurements on experimentally sheared dunites available pre-publication. C. Teyssier is thanked for facilitating the collaboration and scientific discussions. R. Russo and S. Ji are thanked for their careful reviews. During part of this work, A.T. was a postdoctoral fellow at the University of Leeds, UK, funded by the Marie Curie EEC Scholarship ERBC4001GT961583. B.T. was partially funded by NSF-EAR 9628381. [AC]

## References

- [1] N.I. Christensen, The magnitude, symmetry and origin of upper mantle anisotropy based on fabric analysis of ultramafic tectonites, *Geophys. J. R. Astron. Soc.* 76 (1984) 89–112.
- [2] A. Nicolas, N.I. Christensen, Formation of anisotropy in upper mantle peridotites — a review, in: K. Fuchs, C. Froidevaux (Eds.), *Composition, Structure and Dynamics of the Lithosphere–Asthenosphere System*, 16, American Geophysical Union, Washington, DC, 1987, pp. 111–123.
- [3] D. Mainprice, P.G. Silver, Interpretation of SKS-waves using samples from the subcontinental lithosphere, *Phys. Earth Planet. Inter.* 78 (1993) 257–280.
- [4] A. Nicolas, F. Boudier, A.M. Boullier, Mechanism of flow in naturally and experimentally deformed peridotites, *Am. J. Sci.* 273 (1973) 853–876.
- [5] S. Zhang, S. Karato, Lattice preferred orientation of olivine aggregates in simple shear, *Nature* 375 (1995) 774–777.
- [6] A. Vauchez, A. Nicolas, Mountain building: strike-parallel displacements and mantle anisotropy, *Tectonophysics* 185 (1991) 183–201.
- [7] A. Vauchez, G. Barruol, A. Tommasi, Why do continents break up parallel to ancient orogenic belts?, *Terra Nova* 9 (1997) 62–66.
- [8] A. Tommasi, D. Mainprice, G. Canova, Y. Chastel, Viscoplastic self-consistent and equilibrium-based modeling of olivine lattice preferred orientations, 1, Implications for upper mantle seismic anisotropy, *J. Geophys. Res.* (1999) submitted.
- [9] W. Ben Ismail, D. Mainprice, An olivine fabric database: an overview of upper mantle fabrics and seismic anisotropy, *Tectonophysics* 296 (1998) 145–158.
- [10] B. Tikoff, H. Fossen, Three-dimensional deformations and strain facies, *J. Struct. Geol.* (1999) submitted.
- [11] D. Sanderson, R.D. Marchini, Transpression, *J. Struct. Geol.* 6 (1984) 449–458.
- [12] B. Tikoff, H. Fossen, Simultaneous pure and simple shear: the unified deformation matrix, *Tectonophysics* 217 (1993) 267–283.
- [13] C. Truesdell, Two measures of vorticity, *J. Rational Mech. Anal.* 2 (1953) 173–217.
- [14] B. Tikoff, H. Fossen, The limitations of three-dimensional kinematic vorticity analysis, *J. Struct. Geol.* 17 (1995) 1771–1784.
- [15] R.A. Lebensohn, C.N. Tomé, A self-consistent anisotropic approach for the simulation of plastic deformation and texture development of polycrystals: application to zirconium alloys, *Acta Metall. Mater.* 41 (1993) 2611–2624.
- [16] Y.B. Chastel, P.R. Dawson, H.-R. Wenk, K. Bennet, Anisotropic convection with implications for the upper mantle, *J. Geophys. Res.* 98 (1993) 17757–17771.
- [17] G.I. Taylor, Plastic strain in metals, *J. Inst. Met.* 62 (1938) 301–324.
- [18] Q. Bai, S.J. Mackwell, D.L. Kohlstedt, High-temperature creep of olivine single crystals, 1, Mechanical results for buffered samples, *J. Geophys. Res.* 96 (1991) 2441–2463.
- [19] A. Molinari, G.R. Canova, S. Azhy, A self-consistent approach of the large deformation crystal polycrystal viscoplasticity, *Acta Metall.* 35 (1987) 2983–2994.
- [20] M. Kumazawa, O.L. Anderson, Elastic moduli, pressure derivatives, and temperature derivatives of single-crystal olivine and single-crystal forsterite, *J. Geophys. Res.* 74 (1969) 5961–5972.
- [21] D. Mainprice, A FORTRAN program to calculate seismic

- anisotropy from the lattice preferred orientation of minerals, *Comput. Geosci.* 16 (1990) 385–393.
- [22] A. Nicolas, *Structures of Ophiolites and Dynamics of Oceanic Lithosphere*, Kluwer, Dordrecht, 1989, 367 pp.
- [23] H.G. Avé-Lallemant, Mechanisms of preferred orientations in olivine in tectonite peridotites, *Geology* (1975) 653–656.
- [24] B. Tikoff, D. Greene, Stretching lineations in transpressional shear zones: an example from the Sierra Nevada Batholith, California, *J. Struct. Geol.* 19 (1997) 29–40.
- [25] M. Mareschal, R.L. Kellet, R.D. Kurtz, J.N. Ludden, S. Ji, R.C. Bailey, Archean cratonic roots, mantle shear zones and deep electrical anisotropy, *Nature* 375 (1995) 134–137.
- [26] S. Ji, S. Rondenay, M. Mareschal, G. Senechal, Obliquity between seismic and electrical anisotropies as a potential indicator of movement sense for ductile shear zones in the upper mantle, *Geology* 24 (1996) 1033–1036.
- [27] P.E. Wannamaker, A.D. Chave, J.R. Booker, A.G. Jones, J.H. Filloux, Y. Ogawa, M. Unsworth, P. Tarits, R. Evans, Magnetotelluric experiment probes deep physical state of southeastern U.S., *Eos* 77 (34) (1996) 329–333.
- [28] M.K. Savage, P.G. Silver, Mantle deformation and tectonics: constraints from seismic anisotropy in the western United States, *Phys. Earth Planet. Inter.* 78 (1993) 239–244.
- [29] T.A. Stern, J.H. McBride, Seismic exploration of continental strike-slip zones, *Tectonophysics* 286 (1998) 63–78.
- [30] P.G. Silver, Seismic anisotropy beneath the continents: probing the depths of geology, *Annu. Rev. Earth Planet. Sci.* 24 (1996) 385–432.
- [31] G. Helffrich, Lithospheric deformation inferred from teleseismic shear wave splitting observations in the United Kingdom, *J. Geophys. Res.* 100 (1995) 18195–18204.
- [32] D. McNamara, T.J. Owens, P.G. Silver, F.T. Wu, Shear wave anisotropy beneath the Tibetan Plateau, *J. Geophys. Res.* 99 (1994) 13655–13665.
- [33] G. Herquel, Teleseismic shear waves splitting across the Altyn Tagh fault, in: *European Geophysical Society Meeting 62*, European Geophysical Society, Vienna, 1997.
- [34] G. Barruol, P.G. Silver, A. Vauchez, Seismic anisotropy in the eastern United States: deep structure of a complex continental plate, *J. Geophys. Res.* 102 (1997) 8329–8348.
- [35] T.M. Hearn, Anisotropic Pn tomography in the western United States, *J. Geophys. Res.* 101 (1996) 8403–8414.
- [36] R.M. Russo, P.G. Silver, M. Franke, W.B. Ambeh, D.E. James, Shear wave splitting in northeast Venezuela, Trinidad, and the eastern Caribbean, *Phys. Earth Planet. Inter.* 95 (1996) 251–275.
- [37] E. Klosko, F. Wu, H. Anderson, D. Eberhardt-Phillips, J. McElvilly, Shear-wave splitting and seismic anisotropy in the New Zealand region, *Eos* 78 (45) (1997) F488.
- [38] A. Vauchez, G. Barruol, Shear waves splitting in the Appalachians and the Pyrenees: importance of the inherited tectonic fabric of the lithosphere, *Phys. Earth Planet. Inter.* 95 (1996) 127–138.
- [39] G. Barruol, A. Souriau, A. Vauchez, J. Diaz, J. Gallart, J. Tubia, J. Cuevas, Lithospheric anisotropy beneath the Pyrenees from shear waves splitting, *J. Geophys. Res.* (1999) in press.
- [40] D.E. James, M. Assumpção, Tectonic implications of S-wave anisotropy beneath SE Brazil, *Geophys. J. Int.* 126 (1996) 1–10.
- [41] M. Assumpção, S. Lebreton, A. Vauchez, M. Egydio-Silva, A. Tommasi, G. Barruol, Coherent crust and upper mantle deformation around a cratonic core: evidence from surface geology, numerical modeling and seismic anisotropy, in: *Gordon Conference — Interior of the Earth*, Henniker, NH, 1998.
- [42] A. Nicolas, Why fast polarization directions of SKS seismic waves are parallel to mountain belts?, *Phys. Earth Planet. Inter.* 78 (1993) 337–342.
- [43] A. Vauchez, Transpression-induced strain partitioning in the southern Appalachians (USA), in: *Vth International Circumpacific Terrane Conference 42*, *Comunicaciones*, Santiago, 1991, pp. 229–232.
- [44] L. Margheriti, C. Nostro, M. Cocco, A. Amato, Seismic anisotropy beneath the northern Apennines (Italy) and its tectonic implications, *Geophys. Res. Lett.* 23 (1996) 2721–2724.
- [45] L.I. Makeyeva, L.P. Vinnick, S.W. Roecker, Shear-wave splitting and small-scale convection in the upper mantle, *Nature* 358 (1992) 144–147.
- [46] C.J. Wolfe, F.L. Vernon III, Shear-wave splitting at central Tien Shan: evidence for rapid variation of anisotropic patterns, *Geophys. Res. Lett.* 25 (1998) 1217–1220.
- [47] P. Bormann, P.T. Burghardt, L.I. Makeyeva, L.P. Vinnick, Teleseismic shear-wave splitting and deformations in central Europe, *Phys. Earth Planet. Inter.* 78 (1993) 157–166.
- [48] D.I. Doser, R. Yardwood, Strike-slip faulting in continental rifts: examples from Sabukia, East Africa (1928), and other regions, *Tectonophysics* 197 (1991) 213–224.
- [49] K. Theunissen, J. Klerkx, A. Melnikov, A. Mruma, Mechanisms of inheritance of rift faulting in the western branch of the East African Rift, Tanzania, *Tectonics* 15 (4) (1996) 776–790.
- [50] E. Sandvol, J. Ni, S. Ozalaybey, J. Schlue, Shear-wave splitting in the Rio Grande rift, *Geophys. Res. Lett.* 19 (1992) 2337–2340.
- [51] S. Gao, P.M. Davis, H. Liu, P.D. Slack, W. Rigor, Y.A. Zorin, V.V. Mordvinova, V.M. Kozhevnikov, N.A. Logatchev, SKS splitting beneath continental rift zones, *J. Geophys. Res.* 102 (1997) 22781–22797.
- [52] A. Vauchez, G. Barruol, A. Nicolas, Comment on ‘SKS splitting beneath rift zones’, *J. Geophys. Res.* (1999) in press.
- [53] U. Achauer, K.t.w. Group, New ideas on the Kenya rift based on the inversion of the combined dataset of the 1985 and 1989/90 seismic tomography experiment, *Tectonophysics* 236 (1994) 305–329.
- [54] W. Bosworth, M.R. Strecker, Stress field changes in the Afro-Arabian rift system during the Miocene to Recent period, *Tectonophysics* 278 (1997) 47–62.
- [55] A. Nicolas, U. Achauer, M. Daignieres, Rift initiation by lithospheric rupture, *Earth Planet. Sci. Lett.* 123 (1994) 281–298.